Research Article

Optimization and High-Efficiency Photocatalytic Degradation of Petroleum Refinery Wastewater using SiO_2/TiO_2 Nanocomposite under UV Irradiation

Sarmad Abdulrazzaq Rashid* and Wadood Taher Mohammed
Department of Chemical Engineering, College of Engineering, University of Baghdad, Baghdad, Iraq

* Corresponding author. E-mail: sermed1972@fulbrightmail.org
DOI: 10.14416/j.asep.2026.04.011
Received: 29 September 2025; Revised: 10 November 2025; Accepted: 30 December 2025; Published online: 28 April 2026

Abstract
The critical issue of environmental contamination caused by petroleum refinery wastewater (PRW) has attracted significant attention from researchers due to its harmful effects on human health and ecosystems. The real PRW was successfully treated using Silica-Titania (SiO_2/TiO_2, with a weight ratio of 2.5/97.5%) as a novel photocatalyst to remove organic compounds from real wastewater in a newly designed photocatalytic radiation chamber. SiO_2/TiO_2 was prepared by the sol-gel technique and assessed by the XRD, FTIR, FESEM, EDAX, AFM, and BET analysis. Response surface methodology was used to optimize solution pH, catalyst dosage, and reaction time. The results showed that SiO_2/TiO_2 dosage had the most significant impact on the COD reduction efficiency at optimal conditions of pH 3, SiO_2/TiO_2 dosage 2.29 g/L, and time 5.46 h, achieving 94% COD removal and a correlation coefficient of 98.54%, with an energy consumption of 1.719 kWh/L. SiO_2/TiO_2 maintained excellent stability after undergoing five cycles, achieving more than 87.8 % reduction of COD. The outcomes highlighted the synergistic effect between the SiO_2/TiO_2 photocatalyst and the new chamber design, showing significant enhancements in PRW treatment. Despite these promising results, the study was limited to a single PRW sample and a specific UV intensity. The designed photocatalyst can be examined for various wastewater compositions, scale-up feasibility, and long-term operational stability. Finally, the process revealed efficient performance and showed potential to be a cost-effective and eco-friendly approach for COD reduction from PRW.

Keywords: Box-Behnken design, Petroleum refinery wastewater, Photocatalytic degradation, Response surface methodology, SiO_2/TiO_2 nanocomposite

1 Introduction

Environmental concerns in the petroleum industry revolve around wastewater discharged during refinery processes [1]. In Iraq, unit operations such as distillation, thermal cracking, and hydrotreatment generate vast quantities of polluted water, surpassing the volume of processed crude oil by 1.6 times [2]. Consequently, treatment of this wastewater is essential for both reuse purposes and environmental protection. The properties of petroleum refinery wastewater (PRW) vary based on many factors: oil source, production technique, and plant configuration[3]. The effluents contain high concentrations of aromatic and aliphatic contaminants, which pose significant environmental risks [4]. The disposal of the resulting wastewater represents a significant challenge for these refineries. Therefore, it is crucial to adopt a feasible, cost–effective, and eco–friendly approach for treating these effluents [5].

Various methods were adopted to treat refinery and industrial wastewaters, such as chemical oxidation [6], biological approaches [7], electrocoagulation [8], flotation [9], adsorption [10], extraction [11], forward osmosis [12], membrane-based treatments [13] and air plasma treatment [14]. However, most of these methods suffered from low efficiency, and they were incapable of treating low concentrations of contaminants [15]. Moreover, they often resulted in secondary contaminants by shifting pollutants from

one state to another [16]. Biodegradation, as an option, requires extended periods to break down contaminants, and it is not suitable for many pollutants found in PRW [17].

Advanced oxidation processes (AOPs), particularly photocatalysis, have proved to be a highly effective method for refinery wastewater treatment [18] and medical uses, both drug delivery systems [19]and therapy treatments [20]–[23]. The crucial step involves irradiating the semiconductor catalyst to induce photoexcitation. This excitation promotes an electron from the highest occupied energy level (valence band VB) to the lowest unoccupied level at absolute zero (conduction band CB), creating a positive photo–hole in the valence band. The creation of a photoelectron–hole pair is separated by an energy distance referred to as the band gap (E_{bg}). For this process to initiate, the incident light's photon energy must equal or exceed the band gap energy. The electron–hole pair generated may recombine and release heat. At the conduction band, photo–reduction occurs with electron–accepting species, such as oxygen. On the other hand, photo–oxidation occurs in the valence band with electron–donating species, such as hydroxide ions, typically sourced from water. This process produces hydroxyl radicals, which are utilized in breaking down and mineralizing pollutants [24]. Photocatalysis technique offers numerous benefits, including low operational costs, high conversion efficiency and quantum yield, substantial stability and activity, broad applicability in industrial and environmental sectors across a wide pH range, operates at moderate temperatures and pressures, and works at a high range of spectra (UV and visible light), or solar light [25]. However, the process is hindered by recombination, which results in energy dissipation as heat. The photocatalyst's effectiveness increases with the presence of surface species that act as traps by adhering to the photocatalyst surface. Conversely, photoelectron–hole recombination significantly reduces efficiency. Most photocatalysts made from metal oxides have a wide band gap, which reduces their photocatalytic efficiency.

To enhance the effectiveness of these photocatalysts, it is crucial to modify the surface of the photo semiconductor [26]. Semiconductor materials play a crucial role in photocatalytic processes due to their unique combination of electronic structure, light absorption properties, charge transport characteristics, and excited state longevity. The unique electronic configuration of semiconductors, consisting of a filled valence band and an empty conduction band, makes them suitable for use as photocatalysts. Different semiconductors have varying bandgap energies, necessitating different amounts of applied energy to promote electrons from the valence band to the conduction band. When a photon with adequate energy activates a semiconductor, it causes an electron to jump from the filled valence band (lower energy) to the empty conduction band (higher energy). This partially filled conduction band allows the electron to move freely through the semiconductor's crystal structure. Various semiconductors have been studied, including ZrO_2 [27], CuZn, ZnO, ZnS [28], [29], WO_3, CdS, Fe_2O_3, and TiO_2 [18]. Among them, TiO_2 has emerged as the most suitable for widespread environmental applications [30]. Nevertheless, these semiconductors have some limitations that prevent their practical utilization and prompt the demand for developing photocatalysts. Moreover, this environmentally friendly and sustainable approach aligns well with the aim of researchers and industrialists in reaching zero waste production [31].

Titanium dioxide (TiO_2), known for its role as a semiconductor, is commonly used as an effective photocatalyst in water purification processes. It can be obtained and offers several beneficial properties, such as high photocatalytic efficiency, oxidizing potential, and chemical decay resistance in acidic and alkaline environments [32]. Nevertheless, when used alone, TiO_2 has limitations such as a low surface area and the ability for electron (e^-) and hole (h^+) recombination, which diminishes its catalytic performance [33]. As a result, scientists have combined TiO_2 with other materials, such as Graphene oxide [34], chitosan [35], carbon [36], tungsten trioxide [37], bismuth oxide [38], zinc oxide [39], and silicon dioxide [40]. Silicon dioxide (SiO_2) was selected as a composite material for TiO_2 because it can improve photocatalytic efficiency, mechanical strength, thermal stability, and reactive surface area. Furthermore, SiO_2 can enhance the transmission of TiO_2 to the adsorbed molecule by increasing the oxidation potential of its electrons [41]. Silica exhibits excellent adsorption characteristics due to its high surface area. The decomposition of contaminant particles by light exposure on titania can be improved by increasing the surface area. As a result, scientists have investigated the combined technology effects of adsorption and photodegradation on SiO_2/TiO_2 nanocomposites. These materials have revealed improved photocatalytic activity for the light–induced decomposition of all kinds of pollutants

[42]. Despite its numerous advantages, photocatalytic technology has limited adoption in industrial and refinery applications. This is mainly attributed to the low efficiency of photocatalysis when utilizing sunlight and the substantial electricity expenses required for artificial UV lights. To address this issue, significant efforts focused on two main aspects. The first one focuses on improving the catalyst's effectiveness in photocatalysis [43]. This can be accomplished by creating new catalysts, such as nanocomposites, for example, SiO_2 loaded on TiO_2 in optimal amounts. The second aspect includes the design and optimization of photocatalytic reactors [44]. Furthermore, it is crucial to accelerate the development of highly efficient photocatalytic reactors to promote wider industrial application of photocatalytic technology for PRW treatment [45]. Particularly, with the treatment of PRW, because the decomposition of contaminants in PRW requires more time due to the presence of complex organic compounds, which require a highly selective and photoactive catalyst [46].

This study presents an unprecedented technology for treating PRW generated from Iraqi oil refineries using a SiO_2/TiO_2 nanocomposite catalyst that was synthesized via the sol–gel method at a weight ratio of 2.5/97.5% within an AOP system. To our knowledge, this nanocomposite has never been used previously to treat real PRW under realistic operational conditions. This application adds an innovative character to the study, especially with the employment of a newly designed photocatalysis chamber with a unique geometric configuration that enhances photocatalytic efficiency. This study aims to evaluate the system's efficiency in reducing COD from PRW. This is accomplished by examining the effects of key operational variables, such as pH, catalyst dosage, and reaction time, using the response surface methodology (RSM) based on Box–Behnken design (BBD). This approach contributes to improving performance and providing a scalable application model for industrial environments.

2 Materials and Methods

2.1 *Chemicals*

Titanium tetra–isopropoxide (TTIP), 97% pure, served as the titania precursor, while tetraethyl orthosilicate (TEOS), also 97% pure, was used for silica. They were obtained from Merck in Darmstadt, Germany. Ethanol (C_2H_5OH) with 99.9% purity was sourced from Rci Labscan in Bangkok, Thailand. For pH adjustment, hydrochloric acid (HCl) and sodium hydroxide (NaOH), both 99% pure, were acquired from Riedel–de Haen, Germany. Deionized water was utilized for all experimental steps.

2.2 *Synthesis of the catalysts*

Synthesis of Nano–TiO_2 Powder

The synthesis of TiO_2 nanoparticles was achieved through the sol–gel method, as reported in previous work [18]. The first step involved mixing 10 mL of TTIP with 143 mL of C_2H_5OH as a pure solvent. This mixture was then vigorously stirred for 30 min. Then, dropwise addition of 2 M HCl is used to regulate the process hydrolysis and set the pH to 2. Distilled water was then added to the solution, followed by well mixing for 30 min, during which gel formation was observed. The gel was dried at 110 °C for 24 h to eliminate H_2O and organic compounds. Additionally, the powder was calcined at 550 °C for 2 h to produce the desired TiO_2 nanomaterial. This approach was based on the method described by Vijayalakshmi and Rajendran 2012 [47]. The practical steps for preparing the TiO_2 nanoparticles are shown in Figure S1.

Synthesis of Nanocomposite SiO_2/TiO_2

A SiO_2/TiO_2 binary oxide composite was synthesized using a conventional sol–gel method as reported in the previous study [18], with varying ratios of 20, 10, 5, 2.5, 1.25, and 0.0 (bare TiO_2) vol.%. TTIP served as the precursor for Titania and TEOS for Silica, with C_2H_5OH as the solvent. The preparation process started by dissolving TTIP in a mixture of C_2H_5OH and TEOS, followed by 0.5 h of stirring at room temperature. The mixture's pH was adjusted to 3.5 through a dropwise addition of 2M HCl. Distilled water was then added, and the solution was stirred for 0.5 h until the gel was observed. The resulting gel was dried at 110 °C for 24 h and calcined at 550 °C for 2 h. To obtain the SiO_2/TiO_2 nanocomposite, the methodology employed in this research is consistent with approaches described in an earlier study [48]. Figure S2 represents the practical steps related to the preparation of the SiO_2/TiO_2 composite.

2.3 *Design of photoreactor*

A novel, locally designed and constructed photocatalytic reactor inside a radiation chamber was

fabricated at a semi–pilot scale, supporting photocatalysts that can utilize UV irradiation or visible light. The reactor operates in both batch processing and continuous workflow modes. The device comprises a hexagonal–shaped container of stainless steel (32 × 32 × 28 cm) that houses 24 lamps of UV–C (length of 30 cm, width of 2.2 cm, power of 8 W, and wavelength of 254 nm each) externally positioned and purchased from local marketing (Philips, Poland), providing light intensity of 64, 128, and 192 W/m^2 as estimated value based on lamp power and geometry. The selection of lamp type is based on the findings of Joseph *et al*. [49], which evaluated the effectiveness of three UV lamp categories (UV–A, UV–B, and UV–C) in treating wastewater contaminated with methylene blue dye. Their research revealed that UV–C (the shortest wavelength) was the most efficient, achieving complete degradation. Zarei *et al*., study reported identical findings [50]. The illumination lamps are fixed 10 cm from the reactor, forming a reflective plane for incoming radiation. A larger hexagonal cover of industrial wood (46 × 52 × 56 cm) encloses the stainless–steel container. A magnetic stirrer was employed to provide efficient mixing for the reactants in the photoreactor. This new setup of the reactor enhances the mixing of reactants during the reaction, which ensures that catalyst particles are uniformly distributed in the illuminated zone created by the UV lamps. This configuration potentially leads to improved photo–catalytic performance. Two fans were mounted in front of the reactor to supply filtered, cooled air and maintain the internal temperature below 40 °C and dissipate heat generated by the UV irradiation, while a heat sensor connected to an automatic controller regulated the fan operation to ensure temperature stability.

Two additional fans circulated air inside the reactor to prevent hot spots and thermal gradients. A timing mechanism is incorporated to automatically switch off the device after a preset reaction duration, facilitating unattended operation and enhancing safety. To maximize the utilization of UV light, the photo reactor was completely covered by aluminum foil, effectively isolating it from its surroundings. An additional layer of glass wool was applied to ensure perfect insulation. The innovative design of the photoreactor enhances UV lamp utilization, improves catalyst–solution mixing during operation, and facilitates particle separation from the solution through filtration. These features contribute to the reactor's superior photocatalytic activity compared to traditional designs. Figure 1 illustrates the structural setup of the reactor, while Figure S3 represents the photoreactor images.

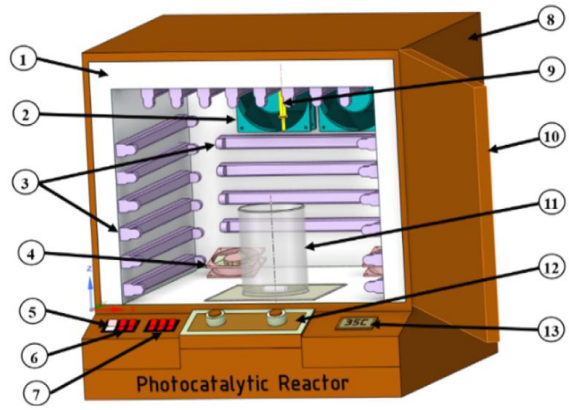

Figure 1: The configuration of the photoreactor including, stainless–steel container (1), cooling fan (2), UV lamps (3), mixing fan (4), on/off button (5), mixing fan button (6), lamps controller (7), wooden external cover (8), temperature sensor (9), the door (10), reactor vessel (11), magnetic stirrer (12), and Temperature controller (13).

2.4 *Procedure*

A 500 mL sample of PRW was placed in a 1000 mL vessel. The photooxidation tests were conducted in a batch photoreactor at many pH values. The solution's pH was adjusted as necessary by adding 1M HCl or NaOH. A specific dosage of photocatalyst (1, 2, and 3 g/L) was added to the solution and well mixed by a magnetic stirrer operating at 250 rpm, keeping a steady temperature of about 25 °C inside the photoreactor. The vessel was placed inside the reactor without any light for 30 min, to create dark conditions and allow adsorption equilibrium between the catalyst particles and the organic compounds [51]. After that, the solution was subjected to UV light using 24 lamps (254 nm wavelength), each 8 W. 2 mL of treated water was taken for analysis at various intervals. The samples were centrifuged and filtered through microfilter paper to remove photocatalyst particles. The Lovibond device was used to measure the COD of the samples [52]. The COD removal was evaluated by calculating the COD reduction percentage and the removal efficiency (RE%) of COD using Equation (1) [53]:

$$RE\ \% = \frac{COD_i - COD_f}{COD_i} x\ 100 \quad (1)$$

Where: COD_i represents the initial concentration of COD in (mg/L), while COD_f denotes the final COD concentration after exposure to light for a duration of t in minutes.

In the photocatalytic process, electrical energy consumption is an essential financial parameter. For this process, Equation (2) illustrates how the Electrical Energy per Order (EE/O) was estimated [54]:

$$EE/O = \frac{P*t}{V*Log(\frac{C_i}{C_f})} \quad (2)$$

Where EE/O is Electrical Energy per Order in kWh/L, P represents the rated power of the UV lamp in kW, t refers to the reaction time (h), and V denotes the volume of solution (L).

2.5 *Characterization and analytical method*

2.5.1 Characterization of petroleum refinery effluents

This study examined 40 L of PRW from the Al–Dora refinery in Iraq. The PRW sample was collected from the tank before the biological treatment unit and stored at 4 ºC in the laboratory refrigerator until use. The characteristics of the PRW, before its treatment through the photocatalytic process, were provided by the plant's management and are presented in Table 1.

Table 1: Characteristics of Al–Dora refinery plant wastewater.

Characteristic	Content	Unit
pH	7.3	-
COD	480	ppm
BOD	82	ppm
TDS	1178	ppm
TSS	310	ppm
TUR	87.3	NTU
Phenol	3.5	ppm
Oil	267.2	ppm
PO_4	0.57	ppm
SO_4	435	ppm
Cl	376	ppm
DO	0.0	ppm

2.5.2 Characterization of the catalyst

The structure and characteristics of the synthesized SiO_2/TiO_2 photocatalyst were analyzed using different analytical methods. X–ray diffraction (XRD) was performed using an Angstrom Advanced Inc ADX2700 diffractometer with Cu-Kα radiation (λ=1.5406Å). The scan range was 2θ = 20°–80°, which allowed identification of the crystalline phases and composition of the catalyst materials. Fourier transform infrared (FTIR) Spectroscopy was used to detect functional groups present on the photocatalyst surface. This was conducted using a Bruker Vector 22 spectrometer in the range 450–4000 cm^{-1}, employing the KBr pellet technique. The sample's morphology was obtained using a field emission scanning electron microscopy (FESEM) device, Inspect F50 (FEI Company, Netherlands), and energy dispersive analysis by X–ray (EDAX) for quantitative analysis of the photocatalysts was conducted by the same device. The catalyst's topography was examined using atomic force microscopy (AFM) with a Core AFM 2023 made by Nanosurf AG, Switzerland. The structural features, including Brunauer–Emmett–Teller (BET) surface area and pore volume, were determined using adsorption–desorption isotherms with N_2 utilizing Thermo Finnigan equipment, USA. The samples were pretreated at a temperature of 368 K for 1 h and 573 K for 3 h in nitrogen before obtaining a standard 5–point BET isotherm at 77 K. All measurements were conducted using a Micromeretics Gemini analyzer, which reads the amount of N_2 introduced to the sample and automatically calculates the BET surface area [55]. Image–J software was used to determine the average particle size of the SiO_2/TiO_2 photocatalyst based on the images obtained from FESEM.

2.5.3 Analytical methods

The COD test, which is considered an accurate method, is commonly used for quantifying organic compounds in PRW. This analysis enables the measurement of waste by determining the overall amount of O_2 required to decompose organic substances and convert them to CO_2 and H_2O. In this study, COD reduction was used as an indicator to assess the effectiveness of the photocatalytic process in eliminating organic contaminants found in PRW. To estimate the COD value according to a standard method (e.g., APHA 5220) [56], 2 mL of wastewater was added to $K_2Cr_2O_7$ as an oxidizer for 2 h at a temperature of 150 ºC in a thermal incubator reactor (Lovibond, RD125). Subsequently, the sample vial was allowed to cool to room temperature, and the COD was measured using a spectrophotometer (MD200, Lovibond). COD percentage removal efficiency was calculated using Equation (1), as

previously mentioned. The pH of the solution was determined using a digital pH meter (STATER 2000, OHAUS Corporation, USA) [57].

2.5.4 Experimental design and statistical analysis

The experimental design employed a scientific approach to maximize the reduction of COD. To optimize the process, the effects of acidity (pH), catalyst dosage (C), and reaction time (T) on COD reduction were studied. The initial variables, their units, and ranges are outlined in Table 2. Box–Behnken design (BBD), a type of response surface method (RSM), was selected for its efficiency and requires only 15 experiments for three variables [58]. This design offers better organization and cost-effectiveness related to similar 3k designs [59]. Table 3 displays the process parameters and their corresponding levels, represented by numerical codes: 1, 0, and -1, respectively. In BBD, the experimental points are distributed equidistantly from the central point on a hypersphere. The number of runs necessary for these designs can be calculated using a specific formula, as noted in Equation (3) [60]:

Table 2: The process variables and ranges in PRW treatment.

Variables	Range in BBD		
Coded levels	Low (-1)	Middle (0)	High (+1)
X_1: pH of solution	3	7	11
X_2: SiO_2/TiO_2 dosage (g/L)	1	2	3
X_3: Reaction time (h)	4	5	6

Table 3: BBD experimental design.

Run Order	Blocks	Coded Value			Real Value		
		X_1	X_2	X_3	pH X_1	Catalyst dosage,g/L X_2	Reaction time, h X_3
1	1	-1	0	1	3	2	6
2	1	0	1	-1	7	3	4
3	1	0	0	0	7	2	5
4	1	0	-1	1	7	1	6
5	1	0	0	0	7	2	5
6	1	1	1	0	11	3	5
7	1	0	0	0	7	2	5
8	1	1	-1	0	11	1	5
9	1	-1	0	-1	3	2	4
10	1	-1	-1	0	3	1	5
11	1	0	1	1	7	3	6
12	1	-1	1	0	3	3	5
13	1	1	0	-1	11	2	4
14	1	1	0	1	11	2	6
15	1	0	-1	-1	7	1	4

$$N = 2\,K(K-1) + Cp \quad (3)$$

Where: N refers to the number of runs, K represents the number of examined parameters, while Cp denotes the number of central points. A quadratic polynomial equation was used to characterize the investigated system. The relationship between operational factors and process response is described by a model represented in Equation (4), as noted by Babajani and Jamshidi [60]:

$$Y = a_0 + \sum a_i x_i + \sum a_{ij} x_i x_j + \sum a_{ii} {x_i}^2 + \varepsilon \quad (4)$$

Where: Y represents the predicted efficiency in removing COD, a_0 is a constant, a_i is the first–order main effect, a_{ij} represents a linear relationship between the input variables of x_i and x_j (i = 1 and 2, j = 1, 2, and 3), while a_{ii} denoted the input variables 2nd order x_i (i = 1, 2, and 3), x_i^2 and $x_i x_j$ represents the quadratic and interaction effects of independent variables, respectively, and ε denotes the equation's remainder. Analysis of variance (ANOVA) was used to examine the importance of each variable in the polynomial equation (equation 4) [61]. The importance level, or *p*–value, was set at 0.05 for the ANOVA. The F–value was described as the statistical importance of the quadratic second–order models. When the estimated F–value is more than its value in the table, the *p*–value will be very small, indicating the significance of the statistical model. The calculated F–value is produced by dividing the regression mean squares (such as

linear, square, and interaction) by the residual mean squares, as clear in equation 5 [62]:

$$F - value = \frac{MSReg}{MSRes} = \frac{SSReg/DFReg}{SSRes/DFRes} \quad (5)$$

Regression degree of freedom ($DF_{Reg.}$) refers to the number of terms minus one, while the residual degrees of freedom ($DF_{Res.}$) is calculated by subtracting the regression degree of freedom from the total degrees of freedom [62]. The experimental design consisted of 15 tests, including 13 primary tests and 2 replications at the central point [63].

3 Results and Discussion

Control experiments were performed under both dark and light conditions to distinguish between adsorption and photocatalytic degradation. The low removal percentage (7%) validates that contaminants degradation occurs mainly through photocatalysis rather than adsorption.

3.1 *Preliminary experiments*

Preliminary runs were conducted to identify the optimal SiO_2 to TiO_2 loading ratio for the COD reduction. The ratio range was chosen between 20% and 0% (0% representing pure TiO_2) based on previous studies [52], [64]. The main parameters were fixed at a 2 g/L catalyst dosage, pH of 7, and time of 5 h. Table S1 presents the impact of the molar ratio on COD removal efficiency. The results showed that the most effective SiO_2/TiO_2 composite ratio was (2.5/97.5%), yielding a 93.12% degradation rate. The decrease in photocatalytic efficiency of TiO_2 when silica content exceeds 2.5% can be attributed to two main factors: (i) TiO_2 is the photoactive agent responsible for photocatalysis, whereas SiO_2 has limited photocatalytic properties. Excessive SiO_2 loading on TiO_2 can cover or block the active surface of TiO_2, decreasing light absorption and the effective transfer of charge carriers, and reducing contaminant degradation at the TiO_2 active sites. (ii) Although SiO_2 increases surface area and porosity and enhances adsorption capacity, a large amount of SiO_2 scatters and reflects light, diminishing the intensity of light reaching the TiO_2 surface, and hindering the generation of reactive electron–hole pairs essential for photocatalytic reactions [65]. This behavior was demonstrated in our previous work [18], which shows that, at a 2.5% silica loading, XRD analysis indicates that the TiO_2 crystalline structure remains well–preserved. BET measurements further demonstrate a notable increase in the catalyst's surface area, which significantly improves the availability of active sites for photocatalytic degradation.

3.2 *Characterization of nanocomposite photocatalyst*

3.2.1 XRD analysis

Figure 2(a) presents the XRD analysis of the SiO_2/TiO_2 composite with an optimal ratio of 2.5:97.5 according to our previous work, which includes the XRD analysis of the composite with various loading ratios [18]. The plot exhibits a notable change in diffraction peak intensities, indicating variations in the materials' crystallinity. The changes in XRD peak intensities are mainly due to the amorphous nature of SiO_2, suppression of TiO_2 crystallinity, lattice strain, and reduction of crystallite size. These combined effects explain why the SiO_2/TiO_2 composite shows weaker or modified peaks compared to pure TiO_2. As illustrated in Figure 2(a), the XRD patterns of this catalyst reveal that the peaks align with anatase phase TiO_2 (JCPDS 21–1272) [64], a notable peak appears at $2\theta = 25.5°$, while the absence of distinct SiO_2 peaks confirms that SiO_2 is present in an amorphous state, which is well–dispersed onto the TiO_2 matrix, resulting in a SiO_2/TiO_2 composite rather than separate crystalline phases. The intimate contact between amorphous SiO_2 and TiO_T nanoparticles improves interfacial interactions, which enhances the efficiency of charge separation and increases the number of surface hydroxyl groups. These hydroxyl groups act as active sites for photocatalytic reactions. Nonetheless, all substances exhibit peaks consistent to d 101, d 004, d 200, d 105, d 211, d 204, d 116, and d 220 at 2θ of 25.5, 38.2, 48.25, 54.5, 55.1, 63.1, 69.2, and 75.3 degrees, respectively, emphasizing that SiO_2/TiO_2 composite material contains TiO_2 exclusively in the anatase phase [66]. The increased presence of SiO_2 particles in the SiO_2/TiO_2 composites results in a higher proportion of amorphous particles, leading to a decrease in crystallinity. These findings support the high performance of the optimal SiO_2/TiO_2 loading ratio (2.5/97.5%). Similar outcomes were reported by previous studies [64], [67]. Thus, the XRD results confirm that the SiO_2/TiO_2 with (2.5/97.5) loading ratio contains anatase TiO_2 with amorphous (well–dispersed) SiO_2 that improves interfacial interactions for enhanced photocatalytic performance.

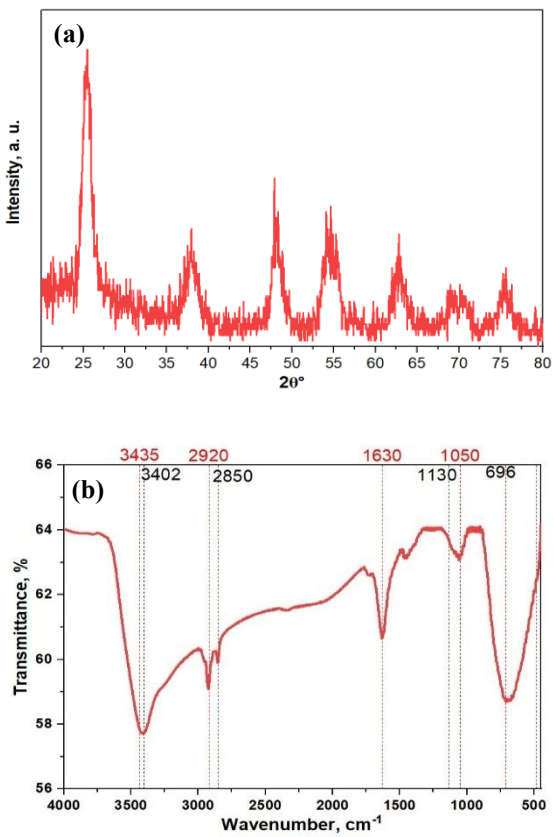

Figure 2: The XRD patterns (a) and FTIR spectra (b) for SiO_2/TiO_2 nanocomposite.

3.2.2 FTIR analysis

FTIR analysis of SiO_2/TiO_2 composites (2.5 /97.5 loading ratio) in the 450–4000 cm^{-1} wavenumber range commonly reveals characteristic functional groups related to silica and titania bonding. Figure 2b illustrates the FTIR spectra of SiO_2/TiO_2 composite with an optimal ratio of 2.5/97.5 according to our previous work, which includes the FTIR spectra of the composite with various loading ratios [18]. The IR absorption bands at 3402–3435 cm^{-1} are characteristic of the stretching vibration of the -OH group. This range typically corresponds to the O-H stretch found in alcohols and other hydroxyl–containing compounds [68], while the 1630 cm^{-1} band represents -OH bending vibration [69]. The O-H stretching of imperfect Si-OH groups and remaining water in the synthesized Si-Ti exhibited a rise in the water band as TiO_2 content increased. The two small infrared bands at 2850 and 2920 cm^{-1} in TiO_2 powders are commonly attributed to residual organic compounds from the precursors used during the preparation process. These organic residues are not eliminated even after washing the TiO_2 powders with distilled water [70]. The peaks at 1050–1130 cm^{-1} generally belong to the asymmetric stretching vibration of the Si-O-Si bond in silicate and silica glass materials [71]. The presence of silica in an amorphous state is typically identified by XRD and FTIR analysis through specific characteristics [52]. Peaks appearing at 657–696 cm^{-1} are aligned with the Ti-O-Ti bond stretching vibration [72]. The variation in O-H intensity between substances indicates that SiO_2 has an active O-H site, which enhances the surface reactions [67].

3.2.3 FESEM and EDAX analysis

The morphological features of the synthesized nanomaterial were investigated using FESEM. Figure 3(a) and (b) displays FESEM images that demonstrate the spherical shape of the SiO_2/TiO_2 nanoparticles. These micrographs also indicate that the nanocomposite consists of mesoporous clusters, with particle aggregation observed, attributed to the amorphous silica content on the surface of TiO_2. These outcomes are consistent with the results of XRD patterns. Siddiqa *et al*., reported similar observations about the SiO_2/TiO_2 photocatalyst [73]. The nanocomposite with a loading ratio of 2.5% SiO_2 to 97.5% TiO_2 exhibited the most favorable result, which is in agreement with a previous study [18]. Image J software analysis confirmed that the SiO_2/TiO_2 particle size was 43.13 nm, supporting the conclusions of numerous researchers in this field [67], [73]. EDAX analysis was utilized to determine the elemental composition of the prepared catalysts. The findings presented in Figure 3(c) correspond with theoretical calculations. The observations about the presence of carbon (C) in the EDX spectrum often originate from the carbon tape used as the sample holder because the sample adhesion during analysis. While nitrogen (N) presence in the EDX spectrum can be explained by the residual surface contamination during the sample preparation process, and the adsorbed nitrogen-containing compounds or intermediates from the treated refinery wastewater, which can remain on the catalyst surface despite the washing process. The elemental mapping is shown in Figure S4. Overall, FESEM images showed that the SiO_2/TiO_2 with a loading ratio (at 2.5/97.5) has spherical shape mesoporous nanoparticles with an average particle size of 43 nm.

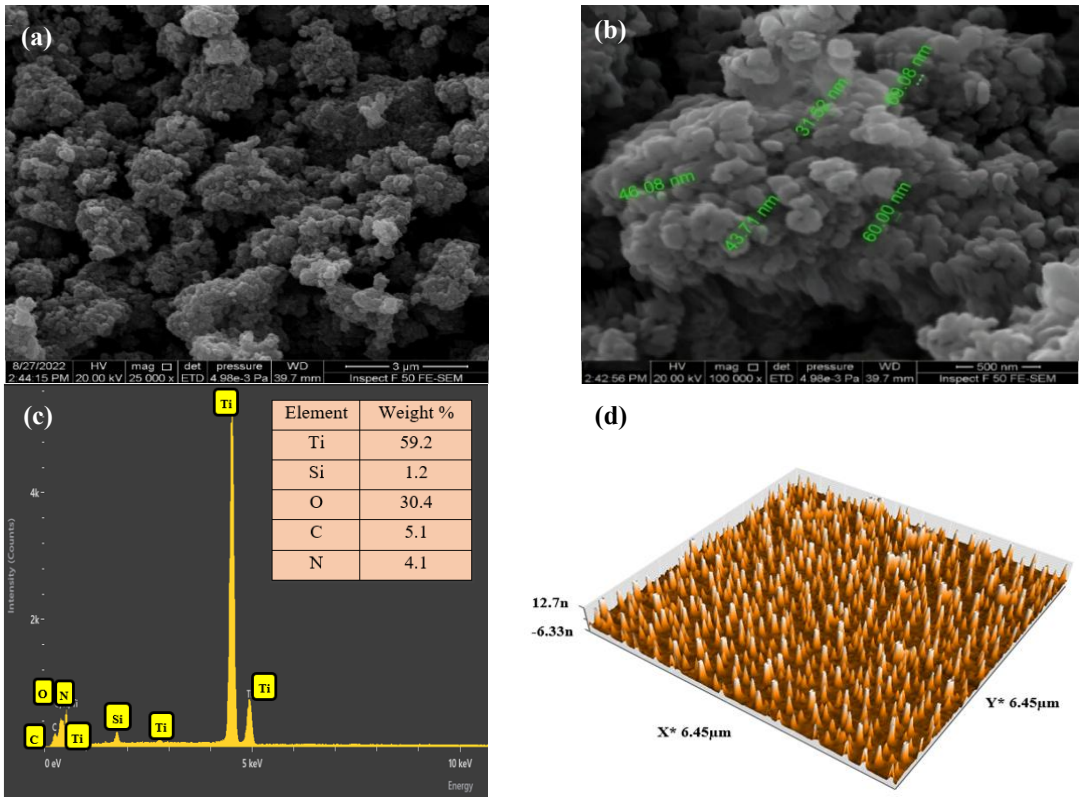

Figure 3: FESEM images for SiO_2/TiO_2 particles (a and b), EDX result (c), and AFM image (d).

3.2.4 AFM analysis

The 3D AFM images, shown in Figure 3(d), exhibited the characteristics of the synthesized SiO_2/TiO_2 photocatalyst surface. The image revealed a uniform particle distribution, with fewer elevations than depressions. AFM generally provided more accurate results of the sample surface characteristics and particle size distribution compared to FESEM.

The average roughness (Sa), root mean square (Sq), skewness values, kurtosis parameter, and average particle diameters are presented in Table S2. The negative values of skewness suggested a left–skewed distribution, indicating a longer left tail. The surface profile with pointed, rounded peaks and sharp valleys corresponds to a high kurtosis measure, confirming the predominance of tall peaks and deep valleys on the surface as found by Khataee *et al*. [74].

3.2.5 BET Analysis

The results showed that pure TiO_2 has a relatively low specific surface area and pore volume of 52.8 m^2/g and 0.08 m^3/g, respectively, while SiO_2/TiO_2 composite with a 2.5/97.5 molar ratio has a high specific surface area and pore volume of 149.21 m^2/g and 0.215 m^3/g, respectively. However, when SiO_2 is loaded on TiO_2, the surface area increases with an excess increase in the silica loading as reported by our previous work for SiO_2/TiO_2 catalysts with different molar ratios [18]. This suggests that incorporating SiO_2 into TiO_2 enhances its surface area, likely due to the textural or structural modifications brought about by the SiO_2 component. The SiO_2/TiO_2 (2.5/97.5%) sample (which represents the optimal ratio) exhibits a higher surface area and satisfactory pore volume, likely due to the enhanced surface area of bare TiO_2. The addition of SiO_2 plays a significant role in maintaining the mesoporosity of the synthesized photocatalyst by prohibiting the collapse of the hole channels, thus providing more sites for photocatalytic degradation [75]. A greater BET surface area is associated with more available sites for photocatalytic reactions, potentially improving oxidation efficiency. This is because a larger surface area exposes more photocatalyst surface to reactants, increasing the

probability of interactions and facilitating the adsorption of reactants onto the catalyst. Moreover, a higher surface area increases light absorption, as well as improving the effectiveness of photocatalytic degradation [76]. Many previous studies reported identical outcomes [66], [70].

3.3 *Statistical analysis of the photocatalytic process results*

The study examined the effects of three key operational variables: solution pH (X_1), photocatalyst dosage (X_2), and reaction time (X_3). These were analyzed using RSM–BBD with the aid of Minitab–22 software. The findings presented in Table 4 reveal that the COD reduction percentage is between 73% to 94%.

Table 4: Optimization results of the photocatalytic process.

Run order	pH X_1	Catalyst dosage, g/L X_2	Reaction time, h X_3	Final COD	RE %	
					Actual	Predicted
1	3	2	6	28	94.0	95.08
2	7	3	4	62	87.0	87.81
3	7	2	5	43	91.0	92.00
4	7	1	6	72	85.0	84.19
5	7	2	5	38	92.0	92.00
6	11	3	5	37	92.2	92.46
7	7	2	5	34	93.0	92.00
8	11	1	5	97	79.7	80.46
9	3	2	4	50	89.5	89.45
10	3	1	5	72	85.0	84.74
11	7	3	6	45	90.5	90.19
12	3	3	5	29	94.0	93.24
13	11	2	4	62	87.0	85.93
14	11	2	6	31	93.5	93.55
15	7	1	4	130	73.0	73.31

Table 5: ANOVA results for COD reduction from PRW.

Source	DF	Seq. SS	Cont. %	Adj. SS	Adj. MS	F–Value	*p*–value
Model	9	482.417	98.54	482.417	53.602	37.58	< 0.001
Linear	3	310.657	63.46	310.657	103.552	72.59	< 0.001
pH (X_1)	1	12.751	2.60	12.751	12.751	8.94	0.030
Conc(g/L)(X_2)	1	210.125	42.92	210.125	210.125	147.30	< 0.001
Time (h) (X_3)	1	87.781	17.93	87.781	87.781	61.54	0.001
Square	3	149.634	30.57	149.634	49.878	34.97	0.001
X_1^2	1	15.013	3.07	7.498	7.498	5.26	0.070
X_2^2	1	112.908	23.06	119.963	119.963	84.10	< 0.001
X_3^2	1	21.713	4.44	21.713	21.713	15.22	0.011
2-Way Interaction	3	22.125	4.52	22.125	7.375	5.17	0.054
X_1*X_2	1	3.062	0.63	3.062	3.062	2.15	0.203
X_1*X_3	1	1.000	0.20	1.000	1.000	0.70	0.441
X_2*X_3	1	18.063	3.69	18.063	18.063	12.66	0.016
Error	5	7.133	1.46	7.133	1.427	–	–
Lack-of-Fit	3	5.133	1.05	5.133	1.711	1.71	0.390
Pure Error	2	2.000	0.41	2.000	1.000	–	–
Total	14	489.549	100.00	–	–	–	–
Model summery	R^2	R^2(adj.)		R^2(pred.)			
	98.45	95.92		82.31			

The findings from the practical experiments can be expressed by a quadratic mathematical model, as illustrated in Equation (6):

$$RE\ \% = -25.5 - 2.625X_1 + 37.02X_2 + 30.94X_3 + 0.089X_1^2 - 5.700X_2^2 - 2.425X_3^2 + 0.219X_1X_2 + 0.125X_1X_3 - 2.125X_2X_3 \quad (6)$$

The negative and positive coefficients indicated that the corresponding terms had diminishing effects. Moreover, these coefficients demonstrated how different factors influenced the result in opposite directions [77]. ANOVA is recognized as a powerful statistical technique for analyzing how a variable behaves as a function of one or more nominal or categorical variables.

This method is employed when it's required to elucidate the distribution of the dependent variable according to measurements of one or more specific independent variables and their different categories (levels). The primary aim of ANOVA is to identify the most crucial weight combinations among the explanatory variables using the F–test (Fisher test), while also assessing the total model reliability [78]. ANOVA was performed for this research, as illustrated in Table 5; the F–value is 37.58. A model's significance is typically determined by a *p*–value probability below 5% and 1% (equivalent to 95%–99% confidence intervals, respectively). The model is deemed significant if the *p*–value is less than 0.05 or 0.01 [79].

In this investigation, the *p*-value of the regression model is notably low (0.001). Moreover, the model is deemed significant at 5%–1% significance levels. R^2–values, which represent the coefficient of correlation, can be utilized to assess the difference between the proposed model and practical results. R–value approaching one indicates the validity of the statistical model [80]. The current study's model achieved an R^2 value of 0.9854, which is considered adequate. Figure 4 reveals that external factors account for 98.5% of the simple difference in RE%. Figure 4 presents the interaction between normal, predicted, and actual charts of the residual based on the practical data for COD reduction using the photocatalytic process. In a normal probability plot, points should generally appear as a straight line, confirming that the expected response values influenced the observed experimental outcomes [81]. As shown in Figure 4a, the experimental data dispersion forms a straight line, indicating a dependency on the values of the anticipated response. The residual versus fits graph, presented in Figure 4b, assesses the consistency of residual variance. The data points exhibit distribution around the horizontal zero line, suggesting reasonable residual variance.

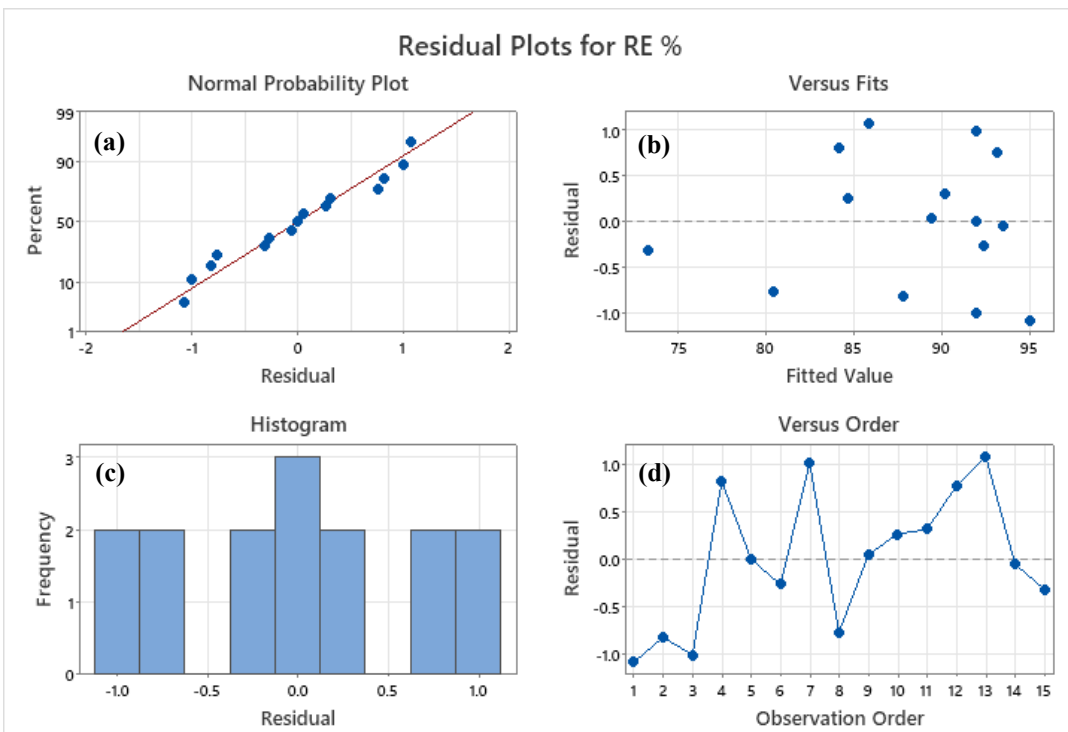

Figure 4: Residual plots for COD removal: (a) Normal probability, (b) Residual versus fitted value, (c) The histogram, and (d) Residual versus observation order.

Figure 4(c) displays a histogram plot demonstrating the dispersion of residuals for all observation points. A bell–shaped curvature in the histogram chart typically indicates a good model fit, and the chart here closely resembles this ideal shape. Figure 4(d) presents the residual versus order plot, which is used to verify the assumption of residual independence. Ideally, the residuals should be randomly distributed around the zero line. The data points in this plot follow a logical pattern, verifying that residuals are indeed independent of each other [82].

3.4 *Effect of variables on the response*

The model equation was used to create three–dimensional surface plots (3D) and two–dimensional contour plots (2D), which helped identify how every variable influenced the predicted outcomes response. The effects of pH levels (3, 7, and 11), SiO_2/TiO_2 concentrations (1, 2, and 3 g/L), and reaction durations (4, 5, and 6 h) on the percentage of COD reduction from PRW were examined. Given that this study marks the first use of SiO_2/TiO_2 catalyst for treating PRW, it becomes necessary to compare this catalyst's performance in removing various other contaminants.

Figure 5(a) and (b) demonstrates the combined effects of SiO_2/TiO_2 dosage and pH on the removal efficiency percentage at the middle value of time (5 h). The response surface plot is shown in Figure 5(a), while Figure 5(b) displays the corresponding contour diagram. The quantity of catalyst employed also impacts the cost of the process. A minimal amount of catalyst requires extended light exposure and long retention time, leading to an expensive process. On the other hand, excessive catalyst amounts are costly and reduce photoactivity because of the increase in solution turbidity. Consequently, estimating the optimal catalyst amount for the system is significant and essential [55]. Figure 5(a) demonstrated that increasing the SiO_2/TiO_2 dosage results in improved COD removal efficiency due to the production of more hydroxyl radicals, which enhances the oxidation process [83]. However, the decrease in RE% beyond 2.5 g/L can be attributed to the effect of solution turbidity, which represents an obstacle to the penetration of light and dissipation of the UV irradiation from reaching the organic compounds in the solution to oxidize them [84]. This trend aligns with previous studies using SiO_2/TiO_2 composite catalysts for phenol degradation and TiO_2 for COD reduction in PRW [85]. The pH effect is significant as SiO_2/TiO_2 is acidic (from the value of pH_{pzc} in our previous work, which is equal to 6.25 [18]), which influences the photocatalyst surface by increasing $^{\bullet}OH$ and improving adsorption [86]. Figure 5(a) shows that the removal efficiency decreases as pH increases. This occurs because acidic conditions promote the production of $^{\bullet}OH$ and OH^- radicals, which react with pollutants and enhance COD degradation. Numerous studies have confirmed the photocatalysis efficiency in eliminating contaminants at low pH values [87]. In PRW treatment processes, Topare *et al*., reported that 3 is the optimal pH to achieve the highest reduction efficiency of COD by bare TiO_2 and composites [88]. The contour plot (Figure 5(b)) indicates that removal efficiencies exceeding 94% can be achieved within a pH range of 3–5 and a SiO_2/TiO_2 dosage range of 1.87–2.88 g/L.

Figure 5(c) and (d) illustrates the effect of SiO_2/TiO_2 quantity and duration on the removal efficiency percentage (RE%) at pH 7. Figure 5(c) presents a plot of the response surface, while Figure 5(d) shows the plot of the corresponding contour. Figure 5(c) demonstrates that increasing time enhanced the COD reduction efficiency to some extent over the period. It was stated that efficient COD reduction requires an optimal contact period between the photocatalyst and light intensity. The findings revealed that RE% rises with time up to 5.45 h, after which no further improvement in COD removal was observed. This could be attributed to several factors: 1) most easily oxidizable contaminants have already been broken down, 2) a dynamic equilibrium may have been established between the pollutant and catalyst, 3) intermediate compounds may have formed, and 4) adsorption–desorption dynamics may be at play. Khalilova *et al*., reported similar results [89].

The contour plot (Figure 5(d)) indicates that COD removal exceeding 90% can be achieved within 4.25–6 h using a SiO_2/TiO_2 dosage between 1.7–3 g/L. Figure 5(e) and (f) depicts the influence of reaction time and pH on the reduction efficiency at a SiO_2/TiO_2 amount of 2 g/L. The response surface plot is shown in Figure 5(e), while Figure 5(f) displays the corresponding contour plot. Figure 5(e) shows that the increase in time leads to an increase in reduction efficiency until it reaches the optimal time as mentioned above. Conversely, raising the pH slightly reduces the RE%, though a minor increase in RE% is observed when the pH exceeds 7. From this behavior, it can be concluded that the effect of pH is

insignificant. The contour plot (Figure 5(f)) indicates that RE% values above 94 can be achieved within a region in which time is (4.8–6 h) and pH is (3–4.8) [84]. The investigation findings on COD reduction efficiency using SiO_2/TiO_2 photocatalyst show that catalyst dosage, pH, and reaction time influence performance. Specifically, the optimal catalyst dosage is between 1.87–2.88 g/L, pH between 3 and 5, and reaction times of 4.25 to 6 h. These optimal conditions increase COD reduction by balancing catalyst availability and achieving efficient light penetration.

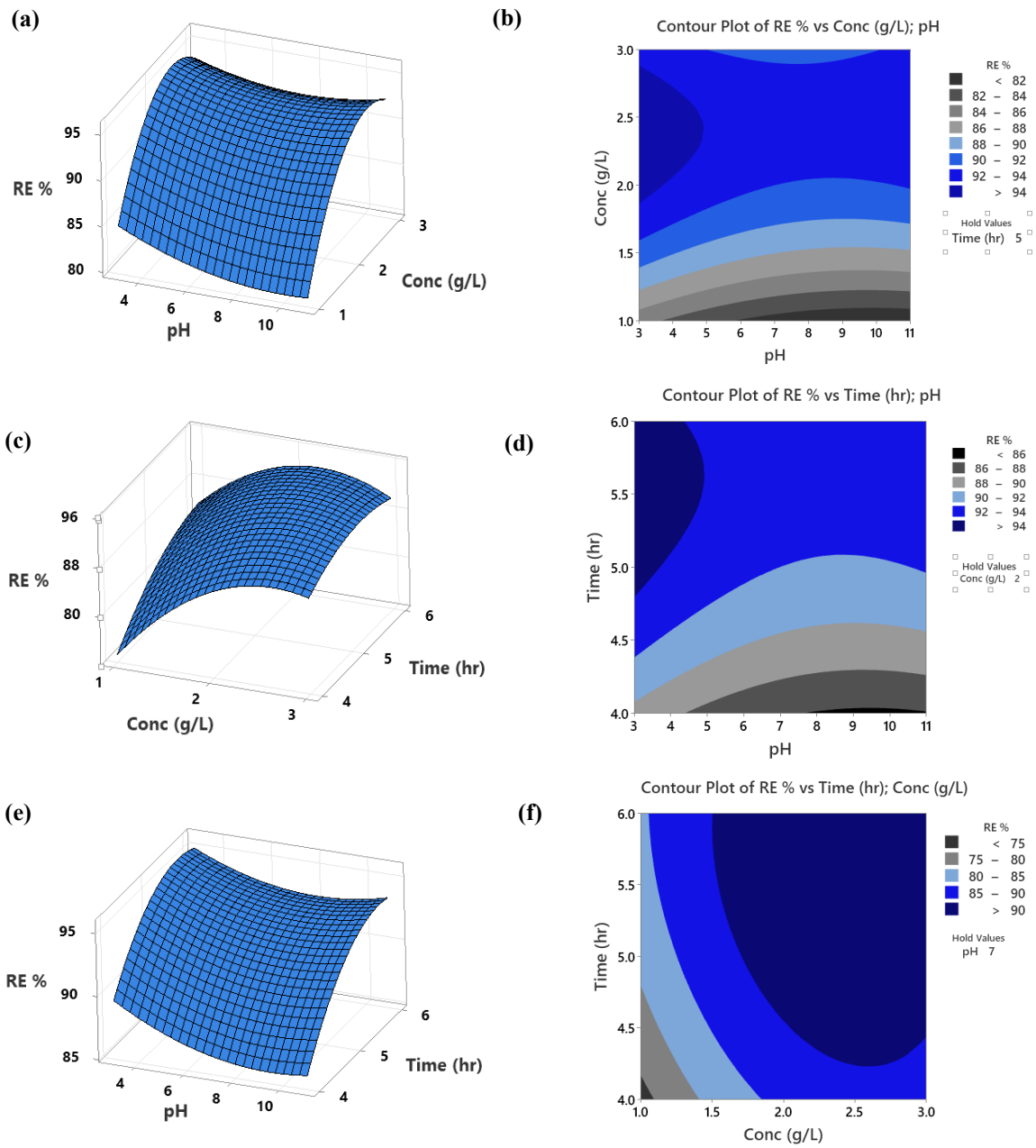

Figure 5: (a) The interaction between pH and SiO_2/TiO_2 dose, (b) contour plot (holding time value of 5 h). (c) The interaction between SiO_2/TiO_2 dose and time, (d) contour plot (holding pH value of 7). (e) The interaction between pH and time, (f) contour plot (hold value SiO_2/TiO_2 dose = 2 g/L).

3.5 *Optimization*

In the optimization processes, the goal is to maximize the response while minimizing energy expenditure. Reduction efficiency was designated as the maximum value, and a desirability function (DF) equal to 1.0. The optimization was conducted using the response optimizer in Minitab 22 software. Table 6 presents the optimization findings. The findings showed that the maximum theoretical removal efficiency is 95.9378%, which can be achieved with a SiO_2/TiO_2 dosage of 2.29 g/L, pH of 3, and reaction time of 5.45 h.

Two confirmation experiments were conducted using the optimum conditions of the parameters as shown in Table S3, and an average maximum COD reduction rate of 94.8% was achieved. The results demonstrated that after 5.45 h of photocatalytic treatment at pH 3, the COD removal efficiency reached 95.94%.

This result corresponds with the optimal value range established by optimization analysis based on the Desirability Function (DF) equal to 1. These findings suggest that the combination of BBD with DF is an effective approach for maximizing COD removal using SiO_2/TiO_2 in the photocatalytic process.

Table 6: Optimization results based on reduction efficiency.

Response	Aimed		Lower	Target	Upper	Weight	Importance
RE (%)	Maximum		73	Maximum	94	1	1
Results				**Parameters**			
SiO_2/TiO_2 (g/L)	pH	Time (h)	RE% Fit	D \F	SE Fit	95% CI	95% PI
2.29	3	5.45	95.94	1	0.79	93.904; 97.972	92.255; 99.621

Table 7: Properties of the wastewater before and after photocatalytic treatment.

Properties	Before	After	Reduction %
pH	7.3	7.1	–
COD (ppm)	480	28	94
BOD (ppm)	82	14	83
TDS (ppm)	1178	820	56
TSS (ppm)	310	35	89
TUR (NTU)	87.3	3.4	96
Phenol (ppm)	3.5	0.021	99.4
Oil (ppm)	267.2	3	98.8
PO4 (ppm)	0.57	0.190	66.6
SO4 (ppm)	435	395	9
Cl (ppm)	376	195	48
DO (ppm)	0.0	4.1	–

Table 7 presents a comparative analysis of the untreated PRW effluent and the effluent after photocatalytic treatment. The table illustrates the differences in characteristics between the initial raw discharge and the final processed output from the photocatalytic system. The findings of this study demonstrate that the treated PRW exhibits superior qualities, with its properties falling within the allowable limits for effluent discharge (COD below 100 ppm). The decrease in turbidity and TSS after photocatalytic treatment can be primarily attributed to physical removal methods like filtration and centrifugation, which effectively remove suspended solids and aggregates produced through the process. Additionally, particle aggregation plays a role due to interactions at the nanoparticle surface and adsorption onto SiO_2/TiO_2 nanoparticles. Consequently, optimization confirmed that high COD reduction (≈95.9%) was obtained with 2.29 g/L SiO_2/TiO_2 dosage, pH of 3, and reaction time of 5.45 h, emphasizing the photocatalytic reduction efficiency.

3.6 *Kinetic study*

The kinetics of photocatalytic reduction of COD are often modeled using a pseudo–first–order kinetic equation, especially when the substrate concentration is relatively low [90]. Equation (7) represents the essential for studying the reaction kinetics. The rate of COD degradation is linearly proportional to its concentration (C) [91]:

$$r = -\frac{dC}{dt} = k_{\text{app}} C \tag{7}$$

k_{app} is the apparent first–order rate constant. After integrating this equation, equation 8 can be obtained:

$$\ln\left(\frac{C}{C_0}\right) = -k_{\text{app}} t \tag{8}$$

Here, C_o is the initial COD, C is the concentration at time t, and the slope from plotting -ln (C_o/C) versus time directly provides the apparent rate constant. k_{app}. The result presented in Figure 6 shows a clear linear relationship between ln (C_o/C) and reaction time for the investigated photocatalysts, confirming that the process follows pseudo–first–order kinetics as described by the Langmuir–Hinshelwood model. The

high correlation coefficients (R^2) of 0.9855 for SiO_2/TiO_2 and 0.9713 for bare TiO_2 indicate a very strong linear relationship between the experimental data and the fitted kinetic models, thereby supporting the validity of the chosen kinetic model. The higher reaction rate constant (k = 0.5455 h^{-1}) observed for the SiO_2/TiO_2 composite compared to bare TiO_2 (k = 0.1367 h^{-1}) can indeed be explained by several synergistic effects, including : (i) Increased surface area, (ii) Suppression of electron–hole recombination, (iii) Effective dispersion of TiO_S.

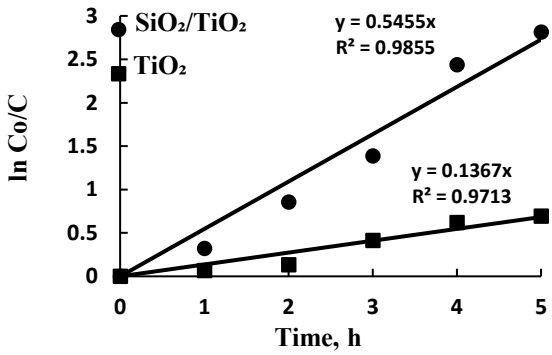

Figure 6: Photocatalytic kinetic model studies for SiO_2/TiO_2 nanocomposite and TiO_2 nanoparticles, under UV irradiation.

3.7 *Reusability of SiO_2/TiO_2 nanocomposite*

The study on the reusability of the SiO_2/TiO_2 nanocomposite photocatalyst shows promising results for its application in photocatalytic oxidation processes. As illustrated in Figure 7, after conducting five cycles of oxidation under fixed conditions (initial COD concentration of 480 mg/L, catalyst dose of 2.29 g/L, pH 3, reaction time of 5.46 h, and UV irradiation), the catalyst maintained a high removal efficiency, decreasing only slightly from 94% to 87.89%. This indicates that the photocatalyst retained most of its activity over repeated uses. The slight decline in catalyst performance is likely due to two factors: (i) a decrease in catalyst mass during the washing step between cycles [92]. (ii) Accumulation of organic pollutant molecules blocking the interior pores of the catalyst, which reduces the number of active sites available for photocatalytic reactions [93].

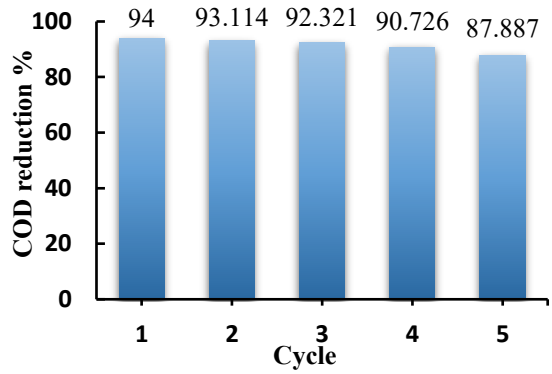

Figure 7: The reusability of SiO_2/TiO_2 photocatalyst.

Despite this minor reduction, the results suggest the SiO_2/TiO_2 nanocomposite exhibits strong reusability and stability in its photocatalytic properties, as represented by reusing the catalyst at least five times. These findings align with similar results reported by other researchers in the field [70], [94].

3.8 *Comparison with previous works*

This study marks the first application of UV/ SiO_2/TiO_2 in treating real PRW, as previous studies primarily focused on utilizing SiO_2/TiO_2 for treating simulated water containing phenol or dyes within photocatalytic AOP. Table 8 compares the COD reduction efficiency, photocatalyst surface area, and conditions of the photocatalytic process with previous studies. The current system exhibited high effectiveness in treating real contaminated water containing numerous complex organic materials, compared with different photocatalysts that were used to treat PRW in previous studies. While the present work achieves a superior COD removal efficiency (94%), it requires a longer reaction time compared to some studies. This is attributed to the complex and recalcitrant nature of the real, non–simulated PRW used in this study, which contains a mixture of pollutants as shown in Table 1, as opposed to single–model pollutants like phenol or dye. The trade–off between high efficiency on a real, complex effluent and reaction time is a key consideration for practical application. Table 8 also illustrates the impact of the specific surface area of the catalyst on the photocatalytic process, displaying varying surface area values for catalysts used in removing different organic contaminants.

Table 8: Comparison of the present work with previous studies for treating PRW by photocatalytic process.

Experimental Conditions	Light Source	Surface Area m^2/g	Reaction ime, h	RE%	Year	Ref.
Using TiO_2 (P25) as a photocatalyst, TiO_2 dosage of 0.1 g/L, pH = 3, and time = 2 h	UV 200–550 nm	ND	2	78	2012	[95]
Using TiO_2 as a photocatalyst, TiO_2 dosage of 2 g/L, airflow rate of 1.04 L/min, and time of 0.5 h	UV–C	50	0.5	66 phenols 81 SOG	2019	[83]
Using TiO_2 (Degussa P25) as a photocatalyst, TiO_2 dosage of 8 g/L, aeration flow of 1.225 L/min, and time of 90 min	UV–C	50	1.5	76 phenols 88 oils	2020	[96]
Using SnO_2 as a photocatalyst, SnO_2 dosage of 0.1 g/L, pH of 3, and time of 99 min	UV–C	29	1.65	73.16 COD	2024	[84]
Using SiO_2/TiO_2 as a photocatalyst, SiO_2/TiO_2 dosage = 2.29 g/L, pH = 3, and time = 5.46 h	UV–C	149.2	5.46	94 COD	2025	Present work

Note : SOG refers to Power Glide SAE40 motor vehicle oil, and Degussa P25 denotes (80% anatase, 20% rutile)

4 Conclusions

This study is the first to demonstrate the highly effective application of a sol-gel synthesized SiO_2/TiO_2 nanocomposite for the treatment of real, complex petroleum refinery wastewater, achieving >94% COD removal under optimized conditions. The synthesized SiO_2/TiO_2 photocatalyst with an optimal composite ratio of 2.5/97.5% was assessed for its photocatalytic dye ffectiveness in treating PRW, resulting in a nanocomposite having an average particle size of 47.92 nm and a surface area of 149.21 m^2/g. The feasibility of SiO_2/TiO_2 nanoparticles photocatalysis in real PRW treatment was investigated and optimized by RSM-BBD. Three operational factors were examined: pH, SiO_2/TiO_2 dosage, and reaction time, along with their interactive effects on the removal efficiency. The optimum conditions (pH of 3, SiO_2/TiO_2 dosage of 2.29 g/L, and reaction time of 5.46 h) gave an optimal RE% of 94% with energy consumption of 1.719 kWh/L. The model's R^2 value of 98.54% indicated a strong correlation between the predicted and experimental results. ANOVA revealed that SiO_2/TiO_2 dosage had the most significant impact on RE% for COD reduction, followed by reaction time and solution pH. The catalyst maintained high stability and reusability after 5 cycles. The outcomes confirmed that the SiO_2/TiO_2 nanocomposite has considerable potential for broad application in wastewater treatment, removal of various pollutants, and COD reduction. Nevertheless, photocatalytic technology has limited applications in industrial and refineries, which can be attributed to the low effectivness at sunlight and the high electricity expenses required for artificial UV lights.

Author Contributions

S.A.R.: investigation, methodology, data curation, writing an original draft, research design, data analysis; W.T.M.: Supervision, investigation, methodology, reviewing and editing, research design, data analysis, project administration. Both authors have read and agreed to the published version of the manuscript.

Conflicts of Interest

The authors declare conflicts of interest.

Declaration of generative AI and AI-assisted technologies in the writing process

The authors utilized the ChatGPT tool to enhance the language and readability of the manuscript.

Appendix A. Supplementary data

Supplementary data to this article can be found online here.

References

[1] S. K. Kamal, Z. M. Mustafa, and A. S. Abbas, "Reaction kinetics and mass transfer of photocatalytic fenton for phenol degradation in a petroleum refinery wastewater," *Tikrit Journal of Engineering Sciences*, vol. 32, no. 1, pp. 1–11, 2025.

[2] M. Jiad and A. H. Abbar, "Treatment of petroleum refinery wastewater by sono fenton process utilizing the in-situ generated hydrogen peroxide," *Al-Khwarizmi Engineering Journal*,

vol. 19, no. 2, pp. 52–67, 2023, doi: 10.22153/kej.2023.04.002.

[3] S. Yadav and S. Kamsonlian, "Progress on the development of techniques to remove contaminants from wastewater: A review," *Applied Science and Engineering Progress*, vol. 16, no. 3, 2023, Art. no. 6729, doi: 10.14416/j.asep.2023.02.001.

[4] S. Jafarinejad and S. C. Jiang, "Current technologies and future directions for treating petroleum refineries and petrochemical plants (PRPP) wastewaters," *Journal of Environmental Chemical Engineering*, vol. 7, no. 5, 2019, Art. no. 103326, doi: 10.1016/j.jece.2019.103326.

[5] M. M. Jiad and A. H. Abbar, "Treatment of petroleum refinery wastewater by an innovative electro-Fenton system: Performance and specific energy consumption evaluation," *Case Studies in Chemical and Environmental Engineering*, vol. 8, 2023, Art. no. 100431, doi: 10.1016/j.cscee.2023.100431.

[6] W. F. Elmobarak, B. H. Hameed, F. Almomani, and A. Z. Abdullah, "A review on the treatment of petroleum refinery wastewater using advanced oxidation processes," *Catalysts*, vol. 11, no. 7, 2021, Art. no. 782, doi: 10.3390/catal11070782.

[7] S. J. Kulkarni, "Biological treatment of petroleum wastewater: A review on research and studies," *International Journal of Petroleum and Petrochemical Engineering*, vol. 2, pp. 17–21, 2016, doi: 10.20431/2454-7980.0202004.

[8] S. M. Al-Jubouri et al., "Multicomponent equilibrium isotherms and kinetics study of Heavy metals removal from aqueous solutions using electrocoagulation combined with mordenite zeolite and ultrasonication," *Applied Science and Engineering Progress*, vol. 18, no. 1, 2025, Art. no. 7484, doi: 10.14416/j.asep.2024.07.011.

[9] O. Hartal et al., "Combined natural flotation and chemical precipitation for the treatment of vegetable oil refinery wastewater," *International Journal of Environmental Science and Technology*, vol. 21, no. 10, pp. 7295–7306, 2024, doi: 10.1007/s13762-024-05470-6.

[10] S. M. Al-Jubouri, H. A. Al-Jendeel, S. A. Rashid, and S. Al-Batty, "Antibiotics adsorption from contaminated water by composites of ZSM-5 zeolite nanocrystals coated carbon," *Journal of Water Process Engineering*, vol. 47, 2022 Art. no. 102745, doi: 10.1016/j.jwpe.2022.102745.

[11] T. Altaee, S. A. Rashid, and M. F. Abdul Jabbar, "Treatment of used lubricant oil by solvent extraction," *Iraqi Journal of Chemical and Petroleum Engineering*, vol. 23, no. 1, pp. 43–50, 2022, doi: 10.31699/ijcpe.2022.1.6.

[12] Z. A. Ibrahim and A. F. Al-Alawy, "Synthesis and characterization of dual functional potassium doped MWCNT composites (K@ Fe_3O_4@ MWCNT and TEG-K/MWCNT) as innovative osmotic agents for forward osmosis processes," *Journal of Molecular Liquids*, vol. 437, 2025, Art. no. 128452, doi: 10.1016/j.molliq.2025.128452.

[13] A. G. Saleem and S. M. Al-Jubouri, "Efficient separation of organic dyes using polyvinylidene fluoride/polyethylene glycol-tin oxide (PVDF/PEG-SnO_2) nanoparticles ultrafiltration membrane," *Applied Science and Engineering Progress*, vol. 17, no. 4, 2024, Art. no. 7523, doi: 10.14416/j.asep.2024.08.001.

[14] S. Ungwiwatkul, M. Jaikua, K. Prasertboonyai, P. Thana, A. Tamman, and K. Matra, "Plasma-activated municipal wastewater (PAMW): Revolutionizing municipal wastewater into high-value liquid fertilizer for duckweed cultivation through air plasma treatment," *Applied Science and Engineering Progress*, vol. 18, no. 3, 2025, Art. no. 7791, doi: 10.14416/j.asep.2025.04.002.

[15] A. S. Adday and S. M. Al-Jubouri, "Developing a versatile visible-light-driven polyvinylidene fluoride/Ag_2O@CRA photocatalytic membrane for efficient treatment of organic pollutants-contained wastewater," *Journal of Water Process Engineering*, vol. 73, 2025, Art. no. 107713, doi: doi.org/10.1016/j.jwpe.2025.107713.

[16] Q. K. Hameed and W. T. Mohammed, "Treatment of wastewater from oil refineries by a combination of electrocoagulation with photocatalytic processes using immobilized nano-zinc oxide photocatalyst," *Journal of Ecological Engineering*, vol. 25, no. 11, pp. 109–123, 2024, doi: 10.12911/22998993/192671.

[17] I. Oller, S. Malato, and J. A. Sanchez-Perez, "Combination of advanced oxidation processes and biological treatments for wastewater decontamination-A review," *Science of the*

Total Environment, vol. 409, no. 20, pp. 4141–4166, 2011, doi: 0.1016/j.scitotenv.2010.08.061.

[18] S. A. Rashid and W. T. Mohammed, "Effective oxidation of phenol compound by silica oxide-titanium dioxide photocatalyst in a well-designed photocatalysis reactor," *Chemistry Africa*, vol. 8, pp. 3773–3788, 2025, doi: 10.1007/s42250-025-01375-0.

[19] Y. Y. Lim, A. M. A. Zaidi, and A. Miskon, "Composing on-program triggers and on-demand stimuli into biosensor drug carriers in drug delivery systems for programmable arthritis therapy," *Pharmaceuticals,* vol. 15, no. 11, 2022, Art. no. 1330, doi: 10.3390/ph15111330.

[20] Y. Y. Lim, A. M. A. Zaidi, M. Haque, and A. Miskon, "Relationship between tumorigenesis, metastasis, immune evasion, and chemoresistance in osteosarcoma therapy," *Journal of Applied Pharmceutical Science*, vol. 14, no. 1, pp. 064–079, 2024, doi: 10.7324/JAPS.2023.149907.

[21] Y. Y. Lim, A. Miskon, A. M. A. Zaidi, M. M. H. M. Ahmad, and M. A. Bakar, "Structural characterization analyses of low brass filler biomaterial for hard tissue implanted scaffold applications," *Materials*, vol. 15, no. 4, 2022, Art. no. 1421, doi: 10.3390/ma15041421.

[22] Y. Y. Lim, A. Miskon, and A. M. A. Zaidi, "Structural strength analyses for low brass filler biomaterial with anti-trauma effects in articular cartilage scaffold design," *Materials*, vol. 15, no. 13, 2022, Art. no. 4446, doi: 10.3390/ma15134446.

[23] Y. Y. Lim, A. Miskon, A. M. A. Zaidi, M. M. H. M. Ahmad, and M. A. Bakar, "Numerical simulation study on relationship between the fracture mechanisms and residual membrane stresses of metallic material," *Journal of Functional Biomaterials*, vol. 13, no. 1, 2022, Art. no. 20, doi: 10.3390/jfb13010020.

[24] N. J. Sadek, S. M. Alradhi, T. M. Albayati, I. K. Salih, and N. Elmi Fard, "Recent developments in petroleum wastewater treatment based on advanced oxidation processes: A review," *Iranian Journal of Chemistry and Chemical Engineering*, vol. 44, no. 4, pp. 1089–1120, 2025, doi: 10.30492/ijcce.2025. 2044930.6870.

[25] K. Rajeshwar, C. R. Chenthamarakshan, S. Goeringer, and M. Djukic, "Titania-based heterogeneous photocatalysis. Materials, mechanistic issues, and implications for environmental remediation," *Pure and Applied Chemistry*, vol. 73, no. 12, pp. 1849–1860, 2001. doi: 10.1351/pac200173121849.

[26] J. R. Bolton, "Solar detoxification," *Solar Energy*, vol. 56, no. 5, 1996, doi: 10.1016/0038-092x(96)81766-x.

[27] S. M. Abbas and S. M. Al-Jubouri, "ZrO_2 nanoparticles filler-based mixed matrix polyethersulfone/cellulose acetate microfiltration membrane for oily wastewater separation," *Applied Science and Engineering Progress*, vol. 18, no. 1, 2025, Art. no. 7599, doi: 10.14416/j.asep.2024.10.001.

[28] Y. Y. Lim, A. M. A. Zaidi, and A. Miskon, "Combining copper and zinc into a biosensor for anti-chemoresistance and achieving osteosarcoma therapeutic efficacy," *Molecules*, vol. 28, no. 7, 2023, Art. no. 2920, doi: 10.3390/molecules28072920.

[29] Y. Y. Lim, A. Miskon, and A. M. Zaidi, "CuZn complex used in electrical biosensors for drug delivery systems," *Materials*, vol. 15, no. 21, 2022, Art. no. 7672, doi: 10.3390/ma15217672.

[30] J. M. Herrmann, M. N. Mozzanega, and P. Pichat, "Oxidation of oxalic acid in aqueous suspensions of semiconductors illuminated with UV or visible light," *Journal of Photochemistry*, vol. 22, no. 4, pp. 333–343, 1983, doi: 10.1016/0047-2670(83)85012-6.

[31] K. T. Amakiri, A. Angelis-Dimakis, and A. R. Canon, "Recent advances, influencing factors, and future research prospects using photocatalytic process for produced water treatment," *Water Science and Technology*, vol. 85, no. 3, pp. 769–788, 2022, doi: 10.2166/wst.2021.641.

[32] M. Besancon et al., "Influence of the porous texture of SBA-15 mesoporous silica on the anatase formation in TiO_2-SiO_2 nanocomposites," *New Journal of Chemistry*, vol. 40, no. 5, pp. 4386–4397, 2016, doi: 10.1039/C5NJ02859K.

[33] S. M. Park et al., "Hybrid CuxO-TiO_2 heterostructured composites for photocatalytic CO_2 reduction into methane using solar irradiation: Sunlight into Fuel," *American Chemical Society Omega*, vol. 1, no. 5, pp. 868–875, 2016, doi: 10.1021/acsomega.6b00164.

[34] G. R. Silva et al., "Photocatalytic modified membranes with dopamine and GO-TiO_2 applied to petroleum refinery wastewater treatment," *Separation and Purification Technology*, vol. 361, 2025, Art. no. 131621, doi: 10.1016/j.seppur.2025.131621.

[35] A. Balakrishnan, K. Gopalram, and S. Appunni, "Photocatalytic degradation of 2,4-dicholoro phenoxya cetic acid by TiO_2 modified catalyst: Kinetics and operating cost analysis," *Environmental Science and Pollution Research*, vol. 28, pp. 33331–33343, 2021, doi: 10.1007/s11356-021-12928-4.

[36] Y. J. O. Asencios, V. S. Lourenco, and W. A. Carvalho, "Removal of phenol in seawater by heterogeneous photocatalysis using activated carbon materials modified with TiO_2," *Catalysis Today*, vol. 388, pp. 247–258, 2022, doi: 10.1016/j.cattod.2020.06.064.

[37] S. Bai et al., "Improvement of TiO_2 photocatalytic properties under visible light by WO_3/TiO_2 and MoO_3/TiO_2 composites," *Applied Surface Science*, vol. 338, pp. 61–68, 2015, doi: 10.1016/j.apsusc.2015. 02.103.

[38] Y. Liu, F. Xin, F. Wang, S. Luo, and X. Yin, "Synthesis, characterization, and activities of visible light-driven Bi_2O_3-TiO_2 composite photocatalysts," *Journal of Alloys and Compounds*, vol. 498, no. 2, pp. 179–184, 2010, doi: 10.1016/j.jallcom.2010.03.151.

[39] R. Ghamarpoor, A. Fallah, and M. Jamshidi, "A review of synthesis methods, modifications, and mechanisms of ZnO/TiO_2-based photocatalysts for photodegradation of contaminants," *American Chemical Society Omega*, vol. 9, no. 24, pp. 25457–25492, 2024, doi: 10.1021/acsomega.3c08717.

[40] P. Miądlicki, P. Rychtowski and B. Tryba, "Coating of expanded polystyrene spheres by -TiO_2 and TiO_2-SiO_2 thin films," *Journal of Materials Research*, vol. 39, pp. 1473–1488, 2024, doi: 10.1557/s43578-024-01319-3.

[41] Y. Cheng, F. Luo, Y. Jiang, F. Li, and C. Wei, "The effect of calcination temperature on the structure and activity of TiO_2/SiO_2 composite catalysts derived from titanium sulfate and fly ash acid sludge," *Colloids and Surfaces A : Physicochemical and Engineering Aspects*, vol. 554, pp. 81–85, 2018, doi: 10.1016/j.colsurfa.2018.06.032.

[42] T. Cetinkaya, L. Neuwirthov, K. Kutlakova, V. Tomasek, and H. Akbulut, "Synthesis of nanostructured TiO_2/SiO_2 as an effective photocatalyst for degradation of acid orange," *Applied Surface Science*, vol. 279, pp. 384–390, 2013, doi: 10.1016/j.apsusc.2013.04.121.

[43] J. Li et al., "Advances in Z scheme semiconductor photocatalysts for the photoelectrochemical applications: A review," *Carbon Energy*, vol. 4, no. 3, pp. 294–331, 2022, doi: 10.1002/cey2.179.

[44] D. Wang et al., "Engineering and modeling perspectives on photocatalytic reactors for water treatment," *Water Research*, vol. 202, 2021, Art. no. 117421, doi: 10.1016/j.watres.2021.117421.

[45] J. Mei, X. Gao, J. Zou, and F. Pang, "Research on photocatalytic wastewater treatment reactors: design, optimization, and evaluation criteria," *Catalysts*, vol. 13, no. 6, 2023, Art. no. 974, doi: 10.3390/cata l13060974.

[46] I. J. Ani, U. G. Akpan, M. A. Olutoye, and B. H. Hameed, "Photocatalytic degradation of pollutants in petroleum refinery wastewater by TiO_2- and ZnO-based photocatalysts: Recent development," *Journal of Cleaner Production*, vol. 205, pp. 930-954, 2018, doi: 10.1016/j.jclepro. 2018.08.189.

[47] R. Vijayalakshmi and V. Rajendran, "Synthesis and characterization of nano-TiO_2 via different methods," *Archives Applied Science Research*, vol. 4, no. 2, pp. 1183–1190, 2012.

[48] N. F. Azlan, S. Akhbar, S. H. Hanipah, and R. W. Sharudin, "A short review on synthesis and characterisation of nano SiO_2/TiO_2 composite for insulation application," *Malaysian Journal of Chemical Engineering and Technology (MJCET)*, vol. 4, no. 2, pp. 155–166, 2021.

[49] C. G. Joseph, Y. H. Taufiq-Yap, G. L. Puma, K. Sanmugam, and K. S. Quek, "Photocatalytic degradation of cationic dye simulated wastewater using four radiation sources, UVA, UVB, UVC and solar lamp of identical power output," *Desalination and Water Treat*, vol. 57, no. 17, pp. 7976–7987, 2016, doi: 10.1080/19443994.2015.1063463.

[50] M. Zarei, A. R. Khataee, R. Ordikhani-Seyedlar, and M. Fathinia, "Photoelectro-Fenton combined with photocatalytic process for degradation of an azo dye using supported TiO_2 nanoparticles and carbon nanotube cathode: neural network modeling," *Electrochimica Acta*, vol. 55, no. 24, pp. 7259–

7265, 2010, doi: 10.1016/j.electacta.2010. 07.050.

[51] A. Hosseini, J. Foroughi, M. Sabzehmeidani, and M. Ghaedi, "Heterogeneous photoelectro-Fenton using ZnO and TiO_2 thin film as photocatalyst for photocatalytic degradation Malachite Green," *Applied Surface Science Advances*, vol. 6, 2021, Art. no. 100126, doi: 10.1016/j.apsadv.2021.100126.

[52] H. Gobara, R. El-Salamony, D. Mohamed, M. Mishrif, Y. Moustafa, and T. Gendy, "Use of SiO_2-TiO_2 nanocomposite as photocatalyst for the removal of trichlorophenol: A kinetic study and numerical evaluation," *Chemistry and Materials Research*, vol. 6, no. 6, pp. 63–82, 2014.

[53] A. N. Kassob and A. H. Abbar, "Treatment of petroleum refinery wastewater by graphite-graphite electro fenton system using batch recirculation electrochemical reactor," *Journal of Ecological Engineering*, vol. 23, no. 10, pp. 291–303, 2022.

[54] H. M. Al-Tameemi, K. A. Sukkar, A. H. Abbar, and Z. K. Kuraimid, "Optimization of photocatalytic process with SnO_2 catalyst for COD reduction from petroleum refinery wastewater using a slurry bubble photoreactor," *Case Studies in Chemical and Environmental Engineering*, vol. 9, 2024, Art. no. 100687, doi: 10.1016/j.cscee.2024.100687.

[55] M. Khraisheh, L. Wu, A. H. Al-Muhtaseb, A. B. Albadarin, and G. M. Walker, "Phenol degradation by powdered metal ion modified titanium dioxide photocatalysts," *Chemical Engineering Journal*, vol. 213, pp. 125–134, 2012, doi: 10.1016/j.cej. 2012.09.108.

[56] E. W. Rice, R. B. Baird, A. D. Eaton, and L. S. Clesceri, *Standard Methods for the Examination of Water and Wastewater*. Washington, DC: American Public Health Association American Water Works Association Water Environment Federation, 2012.

[57] M. M. Jiad and A. H. Abbar, "Efficient wastewater treatment in petroleum refineries: Hybrid electro-fenton and photocatalysis (UV/ZnO) process," *Chemical Engineering Research and Design*, vol. 200, pp. 431–444, 2023, doi: 10.1016/j.cherd.2023.10.050.

[58] A. K. Hassan, M. A. Atiya, and Z. A. Mahmoud, "Photo-Fenton-like degradation of direct blue 15 using fixed bed reactor containing bimetallic nanoparticles: Effects and Box-Behnken optimization," *Environmental Technology & Innovation*, vol. 28, 2022, Art. no. 102907, doi: 10.1016/j.eti.2022.102907.

[59] M. Fathurrahman, A. Zulys, and J. Gunlazuardi, "Kinetic study and optimization of tetramethylthionine chloride photodegradation by iron-perylene MOF with hydrogen peroxide using response surface methodology," *Applied Science and Engineering Progress*, vol. 18, no. 3, 2025, Art. no. 7683, doi: 10.14416/j.asep.2025.02.002.

[60] N. Babajani and S. Jamshidi, "Investigation of photocatalytic malachite green by iridium doped zinc oxide nanoparticles: Application of response surface methodology," *Journal of Alloys and Compounds*, vol. 782, pp. 533–544, 2019, doi: 10.1016/j.jallcom.2018. 12.164.

[61] J. Rumky, M. C. Ncibi, R. C. Burgos-Castillo, A. Deb, and M. Sillanpaa, "Optimization of integrated ultrasonic-Fenton system for metal removal and dewatering of anaerobically digested sludge by Box-Behnken design," *Science of The Total Environment*, vol. 645, pp. 573–584, 2018, doi: 10.1016/j.scitotenv.2018.07.125.

[62] D. C. Montgomery, *Design and Analysis of Experiments*. New York: John Wiley & Sons Inc., 2017.

[63] M. Mohadesi and A. Shokri, "Treatment of oil refinery wastewater by photo-Fenton process using Box–Behnken design method: Kinetic study and energy consumption," *International Journal of Environmental Science and Technology*, vol. 16, no. 11, pp. 7349–7356, 2019, doi: 10.1007/s13762-018-2153-5.

[64] T. N. S. Ho, T. T. Nguyen, T. H. T. Pham, M. T. Ngo, and M. V. Le, "Photocatalytic degradation of phenol in aqueous solutions using TiO_2/SiO_2 composite," *Chemical Engineering Transactions*, vol. 78, pp. 427–432, 2020, doi: 10.3303/CET2078072.

[65] Y. Hendrix, A. Lazaro, Q. Yu, and J. Brouwers, "Titania-Silica composites: A review on the photocatalytic activity and synthesis methods," *World Journal of Nano Science and Engineering*, vol. 5, no. 4, pp. 161–177, 2015, doi: 10.4236/wjnse.2015.54018.

[66] S. Yohi, C. M. Wu, and R. T. Koodali, "A kinetic study of photocatalytic degradation of

phenol over Titania–Silica mixed oxide materials under UV illumination," *Catalysts*, vol. 12, no. 2, 2022, Art. no. 193, doi: 10.3390/catal12020193.

[67] D. R. Eddy et al., "Photocatalytic phenol degradation by silica-modified titanium dioxide," *Applied Sciences*, vol. 11, no. 19, 2021, Art. no. 9033, doi: 10.3390/app11199033.

[68] A. S. Adday and S. M. Al-Jubouri, "Photocatalytic oxidative removal of the organic pollutant from wastewater using recyclable Ag_2O@CRA heterojunction photocatalyst," *Case Studies in Chemical and Environmental Engineering*, vol. 10, 2024, Art. no. 100852, doi: 10.1016/j.cscee. 2024.100852.

[69] T. Degen, M. Sadki, E. Bron, U. Konig, and G. Nenert, "The highscore suite," *Powder Diffraction*, vol. 29, pp. S13–S18, 2014.

[70] M. A. Gatou, E. Fiorentis, N. Lagopati, and E. A. Pavlatou, "Photodegradation of rhodamine B and phenol using TiO_2/SiO_2 composite nanoparticles: A comparative study," *Water*, vol. 15, no. 15, 2023, Art. no. 2773, doi: 10.3390/w15152773.

[71] A. Duran, C. Serna, V. Fornes, and J. M. F. Navarro, "Structural considerations about SiO_2 glasses prepared by sol-gel," *Journal of Non-Crystalline Solids*, vol. 82, no. 1–3, pp. 69–77, 1986, doi: 10.1016/0022-3093(86)90112-2.

[72] Y. D. Hou et al., "N-doped SiO_2/TiO_2 mesoporous nanoparticles with enhanced photocatalytic activity under visible-light irradiation," *Chemosphere*, vol. 72, no. 3, pp. 414–421, 2008, doi: 10.1016/j. chemosphere.2008.02.035.

[73] A. Siddiqa, S. Sabir, S. Hussain, and B. Muhammad, "Highly active mesoporous SiO_2-TiO_2 based nanocomposites for photocatalytic degradation of textile dyes and phenol," *European Journal of Chemistry*, vol. 4, no. 4, pp. 388–395, 2013, doi: 10.5155/eurjchem.4.4.388-395.826.

[74] A. R. Khataee, M. Zarei, and R. Ordikhani-Seyedlar, "Heterogeneous photocatalysis of a dye solution using supported TiO_2 nanoparticles combined with homogeneous photoelectrochemical process : Molecular degradation products," *Journal of Molecular Catalysis A : Chemical*, vol. 338, no. 1–2, pp. 84–91, 2011, doi: 10.1016/j.molcata.2011.01.028.

[75] L. Cui, Y. Song, F. Wang, Y. Sheng, and H. Zou, "Electrospinning synthesis of SiO_2-TiO_2 hybrid nanofibers with large surface area and excellent photocatalytic activity," *Applied Surface Science*, vol. 488, pp. 284–292, 2019, doi: 10.1016/j.apsusc.2019.05.151.

[76] M. M. Jiad and A. H. Abbar, "Petroleum refinery wastewater treatment using a novel combined electro-Fenton and photocatalytic process," *Journal of Industrial and Engineering Chemistry*, vol. 129, pp. 634–655, 2024, doi: 10.1016/j.jiec.2023.09.018.

[77] S. G. Nasab, A. Semnani, A. Teimouri, M. J. Yazd, T. M. Isfahani, and S. Habibollahi, "Decolorization of crystal violet from aqueous solutions by a novel adsorbent chitosan/nanodiopside using response surface methodology and artificial neural network-genetic algorithm," *International Journal of Biological Macromolecules*, vol. 124, pp. 429–443, 2019, doi: 10.1016/j.ijbiomac.2018. 11.148.

[78] P. Ramesh, K. Saravanan, P. Manogar, J. Johnson, E. Vinoth, and M. Mayakannan, "Green synthesis and characterization of biocompatible zinc oxide nanoparticles and evaluation of its antibacterial potential," *Sensing and Bio-Sensing Research*, vol. 31, 2021, Art. no. 100399, doi: 10.1016/j.sbsr.2021.100399.

[79] H. Chaker, A. E. Attar, M. Djennas, and S. Fourmentin, "A statistical modeling-optimization approach for efficiency photocatalytic degradation of textile azo dye using cerium-doped mesoporous ZnO: A central composite design in response surface methodology," *Chemical Engineering Research and Design*, vol. 171, pp. 198–212, 2021, doi: 10.1016/j.cherd.2021.05.008.

[80] H. Derikvandi and A. Nezamzadeh-Ejhieh, "Designing of experiments for evaluating the interactions of influencing factors on the photocatalytic activity of NiS and SnS_2: Focus on coupling, supporting and nanoparticles," *Journal of Colloid and Interface Science*, vol. 490, pp. 628–641, 2017, doi: 10.1016/j.jcis.2016.11.102.

[81] G. E. P. Box and D. W. Behnken, "Some new three level designs for the study of quantitative variables," *Technometrics*, vol. 2, no. 4, pp. 455–475, 1960, doi: 10.1080/00401706.1960.10489912.

[82] M. Rafiee, M. Sabeti, F. Torabi, and A. Rahimbakhsh, "COD reduction of aeration effluent by utilizing optimum quantities of UV/H_2O_2/O_3 in a small-scale reactor," *Processes*, vol. 10, no. 11, 2022, Art. no. 2441, doi: 10.3390/pr10112441.

[83] E. K. Tetteh, D. B. Naidoo, and S. Rathilal, "Optimization of photo-catalytic degradation of oil refinery wastewater using Box-Behnken design," *Environmental Engineering Research*, vol. 24, no. 4, pp. 711–717, 2019, doi: 10.4491/eer.2018.216.

[84] H. M. Al-tameemi, K. A. Sukkar, A. H. Abbar, and Z. K. Kuraimid, "Optimization of photocatalytic process with SnO_2 catalyst for COD reduction from petroleum refinery wastewater using a slurry bubble photoreactor," *Case Studies in Chemical and Environmental Engineering*, vol. 9, 2024, Art. no. 100687, doi: 10.1016/j.cscee.2024.100687.

[85] S. O. Tebbi et al., "green synthesis of sustainable and cost-effective TiO_2-SiO_2-Fe_2O_3 heterojunction nanocomposites for rhodamine B dye degradation under sunlight," *Water*, vol. 17, no. 2, 2025, Art. no. 168, doi: 10.3390/w17020168.

[86] A. Al-Hamdi and M. Sillanpaa, "Photocatalytic activities of antimony, iodide, and rare earth metals on SnO_2 for the photodegradation of phenol under UV, solar, and visible light irradiations," in *Advanced Water Treatment*, 2020, Amsterdam, Netherlands: Elsevier, pp. 129–288, doi: 10.1016/B978-0-12-819225-2.00004-1.

[87] A. M. Abeish, H. M. Ang, and H. Znad, "Photocatalytic removal of pollutants from petroleum refinery effluent," presented at the ICCPGE, Alkhoms, Libya, 2016, vol. 1, pp. 25–30.

[88] N. S. Topare, M. Joy, R. R. Joshi, P. B. Jadhav, and L. K. Kshirsagar, "Treatment of petroleum industry wastewater using TiO_2/UV photocatalytic process," *Journal of the Indian Chemical Society*, vol. 92, no. 2, pp. 219–222, 2015.

[89] H. K. Khalilova, S. A. Hasanova, and F. G. Aliyev, "Photocatalytic removal of organic pollutants from industrial wastewater using TiO_2 catalyst," *Journal of Environmental Protection*, vol. 9, pp. 691–698, 2018, doi: 10.4236/jep.2018.96043.

[90] K. K. Hameed, W. T. Mohammed, and S. J. Mohammed, "Photocatalytic treatment of petroleum refinery wastewater by ZnO nanoparticles immobilized on a concrete substrate," *Iraqi Journal of Chemical and Petroleum Engineering*, vol. 26, no. 3, pp. 113–122, 2025, doi: 10.31699/ijcpe.2025.3.10.

[91] K. M. Abed, B. M. Kurji, S. A. Rashid, and B. A. Abdulmajeed, "Kinetics and thermodynamics of peppermint oil extraction from Peppermint leaves," *Iraqi Journal of Chemical and Petroleum Engineering*, vol. 20, no. 4, pp. 1–6, 2019, doi: 10.31699/ijcpe.2019.4.1.

[92] A. A. Okab and A. I. Alwared, "Photodegradation of tetracycline antibiotic by ternary recyclable Z-scheme g-C_3N_4/Fe_3O_4/Bi_2WO_6/Bi_2S_3 photocatalyst with improved charge separation efficiency: Characterization and mechanism studies," *Environmental Nanotechnology Monitoring & Management*, vol. 19, 2023, Art. no. 100767, doi: 10.1016/j.enmm.2022.100767.

[93] Z. H. Jabbar, S. E. Ebrahim, and S. H. Ammar, "Supported heterogeneous nanocomposites (SiO_2/Fe_3O_4/Ag_2WO_4) for visible-light-driven photocatalytic disinfection against *E. coli*," *Materials Science in Semiconductor Processing*, vol. 141, 2022, Art. no. 106427, doi: 10.1016/j.mssp.2021.106427.

[94] N. M. Bahadur et al., "Ultrasonic assisted synthesis, characterization, and photocatalytic application of SiO_2@TiO_2 core shell nanocomposite particles," *Journal of Nanomaterials*, vol. 2019, no. 1, 2019, Art. no. 6368789, doi: 10.1155/2019/6368789.

[95] J. Saien and F. Shahrezaei, "Organic pollutants removal from petroleum refinery wastewater with nanotitania photocatalyst and UV light emission," *International Journal of Photoenergy*, vol. 2012, 2012, Art. no. 703074, doi: 10.1155/2012/703074.

[96] E. K. Tetteh, S. Rathilal, & D. B. Naidoo, "Photocatalytic degradation of oily waste and phenol from a local South Africa oil refinery wastewater using response methodology," *Scientific Reports*, 2020, Art. no. 8850, doi: 10.1038/s41598-020-65480-5.